

NASA TECHNICAL NOTE



NASA TN D-3083

e. 1

NASA TN D-3083

LOAN COPY: RETI
AFWL CIVIL
KIRTLAND AFB,



OPTIMIZED TURNING-VANE DESIGN FOR AN INTAKE ELBOW OF AN AXIAL-FLOW COMPRESSOR

by S. Z. Pinckney
Langley Research Center
Langley Station, Hampton, Va.

NATIONAL AERONAUTICS AND SPACE ADMINISTRATION - WASHINGTON, D. C.



TECH LIBRARY KAFB, NM



0079925

NASA TN D-3083

OPTIMIZED TURNING-VANE DESIGN FOR AN INTAKE ELBOW
OF AN AXIAL-FLOW COMPRESSOR

By S. Z. Pinckney

Langley Research Center
Langley Station, Hampton, Va.

NATIONAL AERONAUTICS AND SPACE ADMINISTRATION

For sale by the Clearinghouse for Federal Scientific and Technical Information
Springfield, Virginia 22151 - Price \$2.00

OPTIMIZED TURNING-VANE DESIGN FOR AN INTAKE ELBOW
OF AN AXIAL-FLOW COMPRESSOR

By S. Z. Pinckney
Langley Research Center

SUMMARY

The results of the development of an elbow turning-vane design which produces both a high recovery and a uniform distribution at the exit of a 90° intake elbow of an axial-flow compressor are presented. The elbow exit flow angle did not exceed approximately 10° and an average total-pressure loss coefficient between 0.245 and 0.279 was obtained for the elbow inlet Mach number range 0.175 to 0.483.

INTRODUCTION

Space-limited elbows which make sharp corner-like 90° turns are in widespread use in private industry as well as in aircraft. For one important use of elbows, inlet elbow to an axial-flow compressor, a uniform exit flow distribution as well as a high recovery through the elbow are of major importance. The necessity of a uniform flow distribution entering an axial-flow compressor, and therefore leaving the elbow leading to the compressor, is exemplified by premature compressor stall and local hot spots in the flow after compression if the entering flow distribution is nonuniform. The importance of the development of an elbow and an elbow turning-vane design which produces a high total-pressure recovery through the elbow and a uniform flow distribution at the elbow exit has been shown. (See refs. 1 to 4.)

The present report presents the results of the development of a turning-vane design which produces high recovery and a uniform flow distribution at the exit of a 90° intake elbow for an axial-flow compressor. Results for the elbow exit total-pressure recovery and flow angle are discussed.

SYMBOLS

G vane gaps (see fig. 4)
p static pressure

p_t	total pressure
M	Mach number
R	vane radius
R_{ϕ}	maximum vane radius ($R_{\phi} = R$ for conventional row-type straight vanes)
\bar{R}_{ϕ}	average radius, $\frac{R_{\phi,n-1} + R_{\phi,n}}{2}$
$\frac{\Delta p}{(p_t - p)_i}$	static-pressure rise coefficient, $\frac{p_e - p_i}{p_{t,i} - p_i}$
$\frac{\Delta p_t}{(p_t - p)_i}$	loss coefficient, $\frac{p_{t,i} - p_{t,e}}{p_{t,i} - p_i}$
ϕ_{le}	circumferential location of leading edge of a radial vane
ϕ_{te}	circumferential location of trailing edge of a radial vane
Subscripts:	
av	average
e	exit
i	inlet
n	vane number (fig. 3)

APPARATUS

Inlet Elbow

Figures 1 to 4 show the general experimental configuration as well as the important detail physical dimensions of the inlet elbow. Figure 1 shows photographs of the inlet elbow; figure 2, the geometry of the elbow shell; figure 3, the location of the pertinent parts of the experimental apparatus; and figure 4, the radius ratios and area ratios of the vanes and vane passages.

The inlet duct is circular (figs. 1 and 2) and is followed by conical fairings (fig. 2) which convert the circular inlet duct into a rectangle. Extending from the rear wall and out through the elbow exit is a rotor-bearing housing followed by a simulated rotor hub which results in an annular area at the exit of the elbow.

The outer half of the flow entering the elbow (fig. 3) has to pass around the rotor-bearing housing while the inner half has to make a sharp turn of which the inner radius is only 2.55 inches (6.48 cm). A splitter plate (fig. 1(c)) was located on the inlet side of the rotor-bearing housing. The portion of the flow passing around the rotor-bearing housing is turned onto a set of radial vanes by a set of concentric circular vanes (figs. 1(c) and 3) which help turn the flow around the rotor-bearing housing. The radial vanes upon receiving the flow turn it at right angles and out through the annular exit of the elbow.

A series of vane configurations was tested in order to determine the optimum configuration. The vane configuration which had the maximum number of vanes consisted of 22 vanes; vanes 1 to 12 (fig. 3) were conventional row-type straight vanes of constant chord that form quadrants of circular cylinders; vanes 13 to 22 were radial-type vanes that form quadrants of truncated right circular cones whose apexes fall on the rotor center line. The leading edges of all vanes lie in planes parallel to the elbow exit. All vanes were set at approximately 3° positive angle of attack in order to overturn the air slightly. Detail information as to location and leading- and trailing-edge circumferential angles is given in table I; the identification of a, b, c, Φ_{1e} , and Φ_{te} of table I is given in figure 3. Figure 4 (upper plot) shows all the vane passages have a larger exit area (or exit gap) than inlet area (or inlet gap), the vanes on the inner half of the turn (vanes 1 to 12) having the higher values. The asymmetrical area distribution across the elbow was built into the design because it was believed that the turning on the outer half of the elbow would be less efficient than on the inner half and therefore would need a greater number of vanes. Figure 4 (lower plot) also gives the average flow-turning radius \bar{R}_ϕ in terms of inlet gap G_i and exit gap G_e as well as the vane radii R_ϕ in terms of the radius on the inside of the turn, 2.55 inches (6.48 cm). This plot also shows that vane radii and therefore chords (curve of $\frac{R_\phi}{2.55}$) were increased progressively from inside the turn to outside the turn. It will be noted that the ratio $\frac{\bar{R}_\phi}{G_e}$ is on the order of 2.50; this value of radius ratio has been shown by data (ref. 1) to be about optimum for single 90° turns of constant area.

As the tests progressed, variations from the above-mentioned configuration with the maximum number of vanes were tested in order to determine the optimum configuration of vanes. These vane configurations, with the exclusion of the "no-vane" configuration, are listed in table II; configuration 11 differs from configuration 10 only in that an exit nozzle was added.

Air Supply

The tests were conducted with air furnished by a pair of centrifugal compressors in series and in conjunction with a high-pressure air supply. The combined flow capacity of the compressors and the high-pressure air supply was 80,000 cubic feet per minute ($2264 \text{ m}^3/\text{min}$) at a pressure rise of $3/8$ atmosphere; the flow capacity of the centrifugal compressors in series was 40,000 cubic feet per minute ($1132 \text{ m}^3/\text{min}$) at a pressure rise of $3/8$ atmosphere. The combined airflow was pumped into a settling chamber from which a duct passed to the elbow inlet. The airflow was delivered to the inlet reference station at a range of Mach numbers from approximately 0.170 to 0.483 and a range of Reynolds number per foot (per 0.3048 m) of approximately 1.52×10^6 to 3.90×10^6 . The flow through the elbow was discharged directly to the atmosphere.

Instrumentation

An inlet total-pressure tube and four circumferentially equispaced wall static-pressure orifices were located 9.75 (24.77 cm) and 11.38 (28.91 cm) inches, respectively, upstream of the elbow inlet (fig. 3). Exit total pressures and flow angle measurements were made at the elbow exit plane indicated in figure 3. Configurations 10 and 11 had eight exit static-pressure orifices, four on the inner body and four on the exit nozzle (90° apart), located at the station shown in figure 3. Inlet and exit wall static pressures were read from manometers. Survey measurements of radial and circumferential total pressure and flow angles were recorded on electronic data recorders using differential pressure transducers to measure the pressures and an automatic yaw alignment device (ref. 4) to measure the flow angles.

Procedure

The investigation of the inlet flow consisted of total-pressure surveys and wall static-pressure measurements at the inlet elbow stations indicated in figure 3. The inlet total-pressure surveys were conducted perpendicular to the duct wall at several stations around the duct.

The investigation of the exit flow of the inlet elbow began with the tests of the inlet elbow with no turning vanes. Circumferential surveys of total pressure and flow angle were made for circumferential angles from 0° to 180° (fig. 3) at distances of 0.5, 2.5, and 4.0 inches (1.27, 6.35, and 10.16 cm) from the rotor hub wall. After the "no vane" condition, a series of vane configurations were tested; these vane configurations and the type of surveys made are given in table II. The circumferential surveys for the "no vane" condition as well as for the vane configurations indicated in table II were conducted by setting the survey probe at a known radial distance from the rotor hub and revolving the rotor hub and the probe as a unit. The radial surveys indicated in table II were conducted at the circumferential angles stated. The circumferential angles indicated in table II correspond to those of figure 3.

RESULTS AND DISCUSSION

Inlet Flow Distribution

Plots of the inlet flow distribution in terms of dynamic pressure $(p_t - p)_i$ (not presented herein) revealed a uniform flow entering the elbow.

Exit Flow Distribution

The performance of the present inlet elbow and the various vane configurations tested was determined by the use of four parameters,

(1) Local flow-angle values

(2) Local total-pressure loss coefficient, $\frac{\Delta p_t}{(p_t - p)_i}$

(3) Average static-pressure rise coefficient, $\left[\frac{\Delta p}{(p_t - p)_i} \right]_{av}$

(4) Average total-pressure loss coefficient, $\left[\frac{\Delta p_t}{(p_t - p)_i} \right]_{av}$

The local flow-angle values and local total-pressure loss coefficient are obtained from total-pressure and flow-angle surveys. The average total-pressure

loss coefficient $\left[\frac{\Delta p_t}{(p_t - p)_i} \right]_{av}$ was determined for vane configurations 1 to 11

and the no-vane condition by using the following equation:

$$\left[\frac{\Delta p_t}{(p_t - p)_i} \right]_{av} = 1 - \left[\frac{\Delta p}{(p_t - p)_i} \right]_{av} - \frac{(p_t - p)_e}{(p_t - p)_i} \quad (1)$$

For all vane configurations the value of the ratio $\frac{(p_t - p)_e}{(p_t - p)_i}$ was deter-

mined for use in equation (1), the ratio of inlet area to exit area being assumed to produce the theoretical Mach number change with no total-pressure loss through the elbow. Also, for all vane configurations, measured values of elbow inlet total-pressure $p_{t,i}$ and elbow inlet static pressure p_i were utilized. A numerical average of the static-pressure values obtained from the eight exit static-pressure orifices of vane configurations 10 and 11 was used for the exit static pressure for all vane configurations.

No-vane condition.- The contours of local total-pressure loss coefficient $\frac{\Delta p_t}{(P_t - P)_i}$ shown in figure 5(a) show high total-pressure loss regions on the outer wall from the 30° circumferential angle to the 60° circumferential angle and over most of the annulus on the lee side of the rotor-bearing housing (120° to 180°). At the inlet Mach number of approximately 0.25, maximum values of local total-pressure loss coefficient were approximately 1.50 and values of average static-pressure rise coefficient were on the order of 1.20. Figure 6 shows the values of average total-pressure loss coefficient to be approximately 0.775. The exit flow distribution, average static-pressure rise coefficient, and average total-pressure loss coefficient indicate a definite need for turning vanes.

Configurations 1 and 2.- For configuration 1 (table I), vane numbers 1 to 12 were installed in the elbow in the positions indicated in figure 3 with the expectation that improvement of the flow conditions on the inside of the turn would result in improvements on the outside as well. This was not the case, however, as revealed by the local total-pressure loss coefficient contours (fig. 5(b)). Therefore, in order to improve the performance on the lee side of the rotor-bearing housing, radial vanes 13 to 22 were installed in the positions indicated in figure 3; this configuration is designated configuration 2. Upon the introduction of the radial vanes, a radical improvement in elbow performance was evident from comparison of figures 5(b) and 5(c). In comparison with vane configuration 1, the average total-pressure loss coefficient of configuration 2 is reduced from 0.63 to 0.35 (fig. 6) and the average static-pressure rise coefficient is reduced from 1.04 to approximately 0.77. Figure 5(c) shows the local total-pressure loss coefficient values on the lee side of the rotor-bearing housing to be reduced by as much as 1.0. Large values of loss coefficient are still present in the region of the splitter plate or 0° circumferential angle and the first five vanes seem to be producing large losses.

Configurations 3 and 4.- In vane configuration 3, vane numbers 1 to 5 were removed as these vanes were believed to be causing flow blockage. Many of the high values of local loss coefficient in the region of vanes 1 to 5 were thus eliminated (fig. 5(d)) and the values of the average total-pressure loss (fig. 6) and average static-pressure rise coefficients were reduced by approximately 0.10. The $2\frac{1}{2}$ -inch (6.35-cm) survey (fig. 5(d)) shows a thick boundary layer on the splitter plate (0° circumferential angle) and the 4-inch (10.16-cm) survey shows high values of local loss coefficient just off the splitter plate.

For vane configuration 4, in conjunction with the removal of vanes 1 to 5, a large amount of the leading portion of the splitter plate was arbitrarily removed. High values of local loss coefficient were absent from the new configuration (configuration 4) at the $2\frac{1}{2}$ -inch (6.35-cm) survey position but the region of high values of local loss coefficient was increased at the 4-inch (10.16-cm) survey position (dashed curve in fig. 5(d)). The resulting average total-pressure loss coefficient was approximately doubled relative to vane configuration 3 and a definite reason for the doubling is not known. It is believed that the lack of improvement of the flow distribution at the 4-inch

(10.16-cm) survey position was due to the fact that the splitter plate might have furnished a path for the flow of boundary layer from the high-pressure region on the outside of the elbow turn to the low-pressure region on the inside of the elbow turn; therefore, by removing a large amount of the leading portion of the splitter plate, this path was broken and a total-pressure deficiency appeared that had not existed before. The total-pressure deficiency on the inside of the turn (0° circumferential angle) suggested the possibility of the existence of flow separation. In a previous investigation by the author, a single turning vane located at an optimum position close to the inside of the turn was used to resolve a similar separation problem (ref. 4).

Configurations 5 to 9.- In vane configurations 5 to 9, the effects of vane and elbow shell intersection, end plates, chord length, and leading-edge gap were investigated for the special vane located close to the inside of the elbow turn; this special vane replaced vanes 1 to 5. It was found necessary to have end plates on the special vane in order to act as supports for the vane, to eliminate its odd intersection with the elbow shell, and to eliminate flow of boundary layer from the elbow shell on to the special vane. The chord chosen for the special vane consisted of the 90° arc of a vane which had a 2.66-inch (6.76-cm) radius. The trailing edge of the vane was fixed at 2 inches (5.08 cm) from the elbow wall and from a plot of average static-pressure rise coefficient the optimum leading-edge gap was found to be $1\frac{1}{8}$ inches (2.86 cm) (fig. 7).

Configuration 10.- For vane configuration 10 the optimized special vane as determined in vane configurations 5 to 9 was installed. Total-pressure loss coefficient contours (fig. 5(e)) show low values of local total-pressure loss coefficient up to 4.0 inches (10.16 cm) from the inner wall, and at the 4-inch (10.16-cm) survey position a small region exists with a value of local loss coefficient of approximately 2.0.

Configuration 11.- A check of the improvement of the elbow exit flow distribution of vane configuration 10 was done under exit conditions similar to those of the elbow of reference 4; this elbow configuration is designated configuration 11. Specifically, an exit nozzle scaled to that of reference 4 was installed for configuration 11. The local total-pressure loss coefficient contours of configuration 11 (figs. 5(f) and 5(g)) show an improvement of the local loss coefficient at the 4-inch (10.16-cm) survey position. Figures 5(f) and 5(g), which present data obtained at inlet Mach numbers of 0.302 and 0.424, respectively, show a maximum value of approximately 0.850 for the local loss coefficient at the 4-inch (10.16-cm) position. The values of average static-pressure rise coefficient and average total-pressure loss coefficient for vane configurations 10 and 11 were found to coincide and thus are plotted together in figures 8 and 9 without any means of distinction as to configuration number.

A noticeable fact of interest is the high value of loss coefficient obtained for all elbow configurations at the 4-inch (10.16-cm) survey position and the region of the special vane (circumferential angle of approximately 40°). As this region, 4-inch (10.16-cm) survey and 40° circumferential angle position, had high values of total-pressure loss coefficient for all configurations of the inlet elbow that were tested, it is believed that the elbow shell shape is its cause.

Flow-angle surveys at the exit of the elbow for configuration 11 showed a general underturning of the flow. For an elbow inlet Mach number of 0.424, the general underturning was from 6° to 8° for all survey positions 0.75 (1.91 cm), 2.5 (6.35 cm), and 4.0 inches (10.16 cm) from the inner wall. This condition is a considerable improvement over the elbow presented in reference 4 which had exit flow angles up to a magnitude of 30° .

CONCLUDING REMARKS

A vane configuration was developed for an elbow similar to the space-limited inlet elbows of some axial-flow compressors. After optimization the resulting vane configuration gave a uniform exit flow distribution, an exit flow angle not exceeding approximately 10° , and an average total-pressure loss coefficient between 0.245 and 0.279 for the inlet Mach number range 0.175 to 0.483.

Langley Research Center,
National Aeronautics and Space Administration,
Langley Station, Hampton, Va., July 8, 1965.

REFERENCES

1. Wilbur, Stafford W.: An Investigation of Flow in Circular and Annular 90° Bends With a Transition in Cross Section. NACA TN 3995, 1957.
2. Henry, John R.: Design of Power-Plant Installations. Pressure-Loss Characteristics of Duct Components. NACA WR L-208, 1944. (Formerly ARR L4F26.)
3. Valentine, E. Floyd; and Copp, Martin R.: Investigation To Determine Effects of Rectangular Vortex Generators on the Static-Pressure Drop Through a 90° Circular Elbow. NACA RM L53G08, 1953.
4. Pinckney, S. Z.: Use of a Single Turning Vane to Eliminate Flow Separation in a Space-Limited 90° Intake Elbow of an Axial-Flow Compressor. NASA TM X-1110, 1965.

TABLE I.- VANE DIMENSIONS AND LOCATIONS

[R and a, b, c, Φ_{le} , and Φ_{te} are shown in fig. 3]

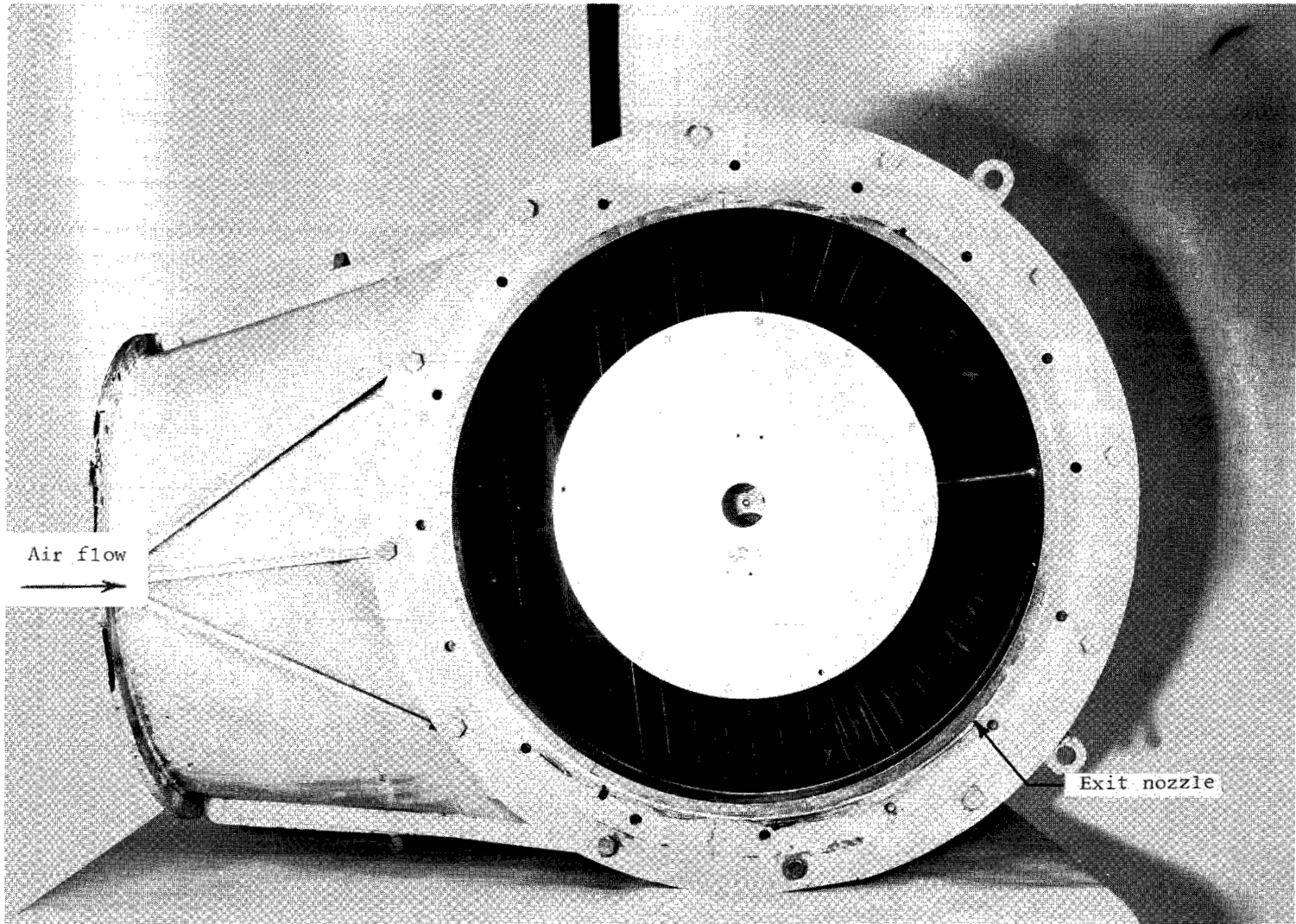
Vane	R (*)		a		b		c		Φ_{le} , deg	Φ_{te} , deg
	in.	cm	in.	cm	in.	cm	in.	cm		
Special vane	2.66	6.76	1.125	2.86	2.00	5.08	2.250	5.72		
**1	2.60	6.60	.442	1.12	1.034	2.63	1.120	2.84		
**2	2.66	6.76	.838	2.13	2.088	5.30	2.118	5.38		
**3	2.72	6.91	1.422	3.61	3.164	8.04	3.136	7.97		
**4	2.82	7.16	1.898	4.82	4.266	10.84	4.154	10.55		
**5	2.88	7.32	2.552	6.48	5.404	13.73	5.224	13.27		
6	2.94	7.47	3.178	8.07	6.516	16.55	6.241	15.85		
7	3.00	7.62	3.693	9.38	7.687	19.52	7.420	18.85		
8	3.10	7.87	4.176	10.61	8.937	22.70	8.531	21.67		
9	3.16	8.03	4.801	12.19	10.233	25.99	9.656	24.53		
10	3.24	8.23	5.488	13.94	11.436	29.05	10.913	27.72		
11	3.30	8.38	6.221	15.80	12.787	32.48	12.163	30.89		
12	3.36	8.53	7.087	18.00	14.107	35.83	13.468	34.21		
13	4.891	12.42	8.040	20.42					87.49	106.01
14	5.033	12.78	9.025	22.92					94.40	113.36
15	5.175	13.14	10.040	25.50					101.59	120.91
16	5.323	13.52	11.087	28.16					108.88	128.68
17	5.466	13.88	12.165	30.90					116.44	136.67
18	5.609	14.25	13.275	33.72					124.21	144.88
19	5.752	14.61	14.400	36.58					132.20	153.30
20	5.895	14.97	15.556	39.51					140.39	161.93
21	6.038	15.34	16.743	42.53					148.80	170.78
22	6.178	15.69	17.978	45.66					157.59	179.6
Wall			18.025	45.78						

*Accuracy of values given for R is ± 0.03 in. (0.0762 cm).

**These five vanes removed for final vane configuration.

TABLE II.- EXPERIMENTAL VANE CONFIGURATIONS

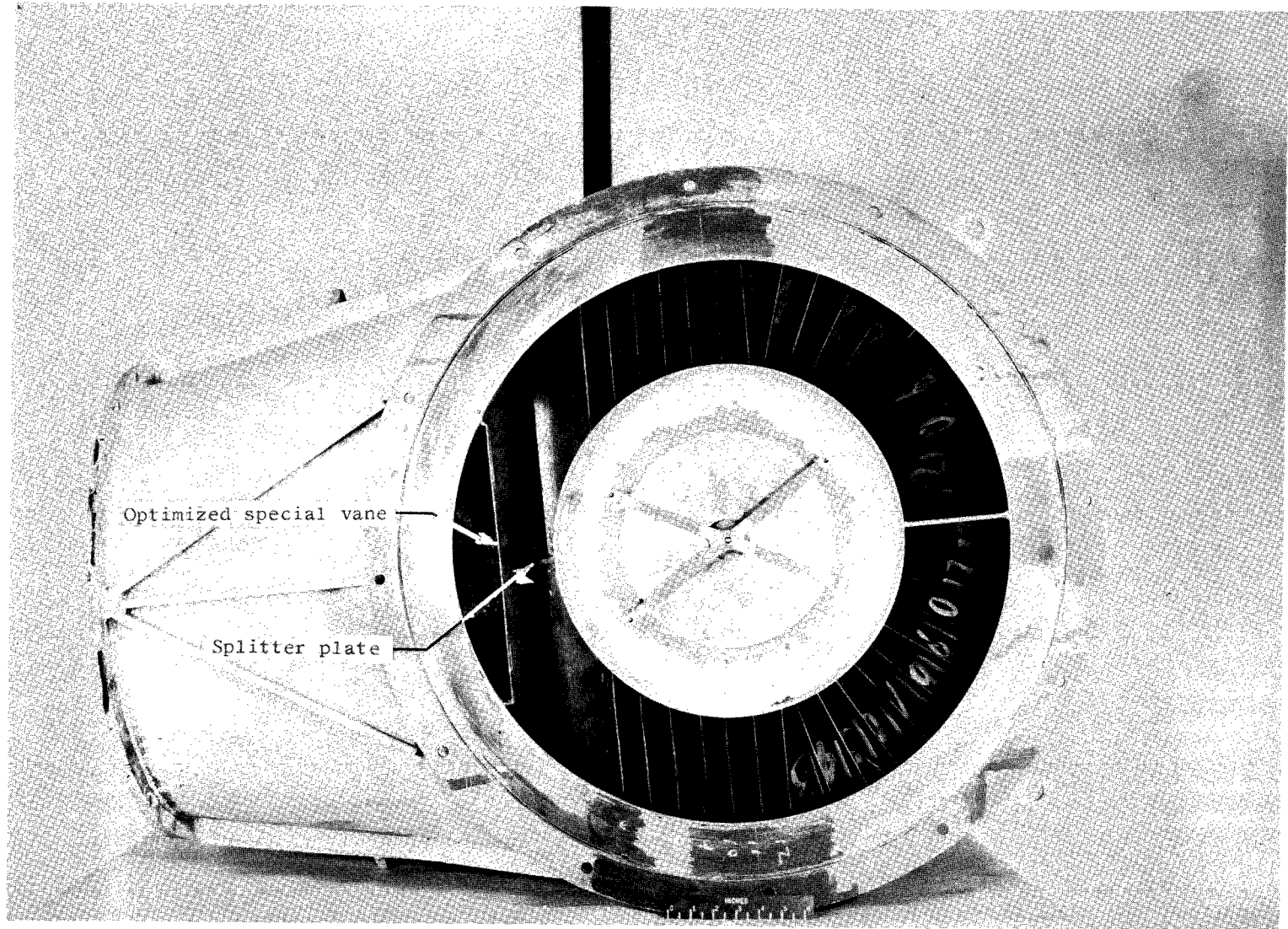
Configuration	Arrangement	Types of circumferential surveys conducted	Circumferential angles of and types of radial surveys conducted	Radial location of circumferential surveys
1	Straight vanes 1 to 12 on inner half of elbow	Total-pressure and flow-angle surveys from 0° to 180° circumferential angle		0.5 inch (1.27 cm), 2.5 inches (6.35 cm), and 4 inches (10.16 cm) from rotor hub
2	Straight vanes 1 to 12 and radial vanes 13 to 22	Total-pressure and flow-angle surveys from 0° to 180° circumferential angle		0.5 inch (1.27 cm), 2.5 inches (6.35 cm), and 4 inches (10.16 cm) from rotor hub
3	Straight vanes 6 to 12 and radial vanes 13 to 22	Total-pressure and flow-angle surveys from 0° to 180° circumferential angle		0.5 inch (1.27 cm), 2.5 inches (6.35 cm), and 4 inches (10.16 cm) from rotor hub
4	Straight vanes 6 to 12 and radial vanes 13 to 22 and splitter plate cut back	Total-pressure and flow-angle surveys from 0° to 180° circumferential angle		0.5 inch (1.27 cm), 2.5 inches (6.35 cm), and 4 inches (10.16 cm) from rotor hub
5	Vanes 6 to 22 and splitter plate cut back and special vane installed	Total-pressure and flow-angle surveys from 0° to 360° circumferential angle		0.75 inch (1.91 cm), 2.5 inches (6.35 cm), 4.0 inches (10.16 cm), and 4.5 inches (11.43 cm) from rotor hub
6	Vanes 6 to 22 and splitter plate cut back and special vane cut off on ends with flat plates on ends as supports	Total-pressure and flow-angle surveys from 0° to 360° circumferential angle		0.75 inch (1.91 cm), 2.5 inches (6.35 cm), 4.0 inches (10.16 cm), and 4.5 inches (11.43 cm) from rotor hub
7	Vanes 6 to 22 and splitter plate cut back and special vane cut off on ends and chord shortened by cutting of trailing 30° of 90° chord	Total-pressure and flow-angle surveys of 111.6° circumferential angle		0.75 inch (1.91 cm), 2.5 inches (6.35 cm), 4.0 inches (10.16 cm), and 4.5 inches (11.43 cm) from rotor hub
8	Vanes 6 to 22 and splitter plate cut back and a variable positioned special vane with ends cut off	Total-pressure and flow-angle surveys of 111.6° circumferential angle	Total-pressure and flow-angle surveys at 0°, 20°, and 30° circumferential angles. Surveys were from 0.25 inch (0.64 cm) to 4.5 inches (11.43 cm) from rotor hub	0.75 inch (1.91 cm), 2.5 inches (6.35 cm), 4.0 inches (10.16 cm), and 4.5 inches (11.43 cm) from rotor hub
9	Vanes 6 to 22 and stationary special vane whose leading edge is $\frac{1}{8}$ inches (2.86 cm) from inner wall with 1/2 inch cut off ends	Total-pressure surveys of 111.6° circumferential angle		0.75 inch (1.91 cm), 2.5 inches (6.35 cm), 4.0 inches (10.16 cm), and 4.5 inches (11.43 cm) from rotor hub
10	Vanes 6 to 22 and flat plates installed on ends of cut-off special vane whose leading edge is $\frac{1}{8}$ inches (2.86 cm) from inner wall and diffuser was added	Total-pressure surveys from 0° to 180° circumferential angle		0.75 inch (1.91 cm), 2.5 inches (6.35 cm), 4.0 inches (10.16 cm), and 4.5 inches (11.43 cm) from rotor hub
11	Same as configuration 10 except that an exit nozzle was added	Total-pressure and flow-angle surveys from 0° to 180° circumferential angle		0.75 inch (1.91 cm), 2.5 inches (6.35 cm), 4.0 inches (10.16 cm), and 4.5 inches (11.43 cm) from rotor hub



(a) Downstream end of elbow; exit nozzle installed.

L-58-909.1

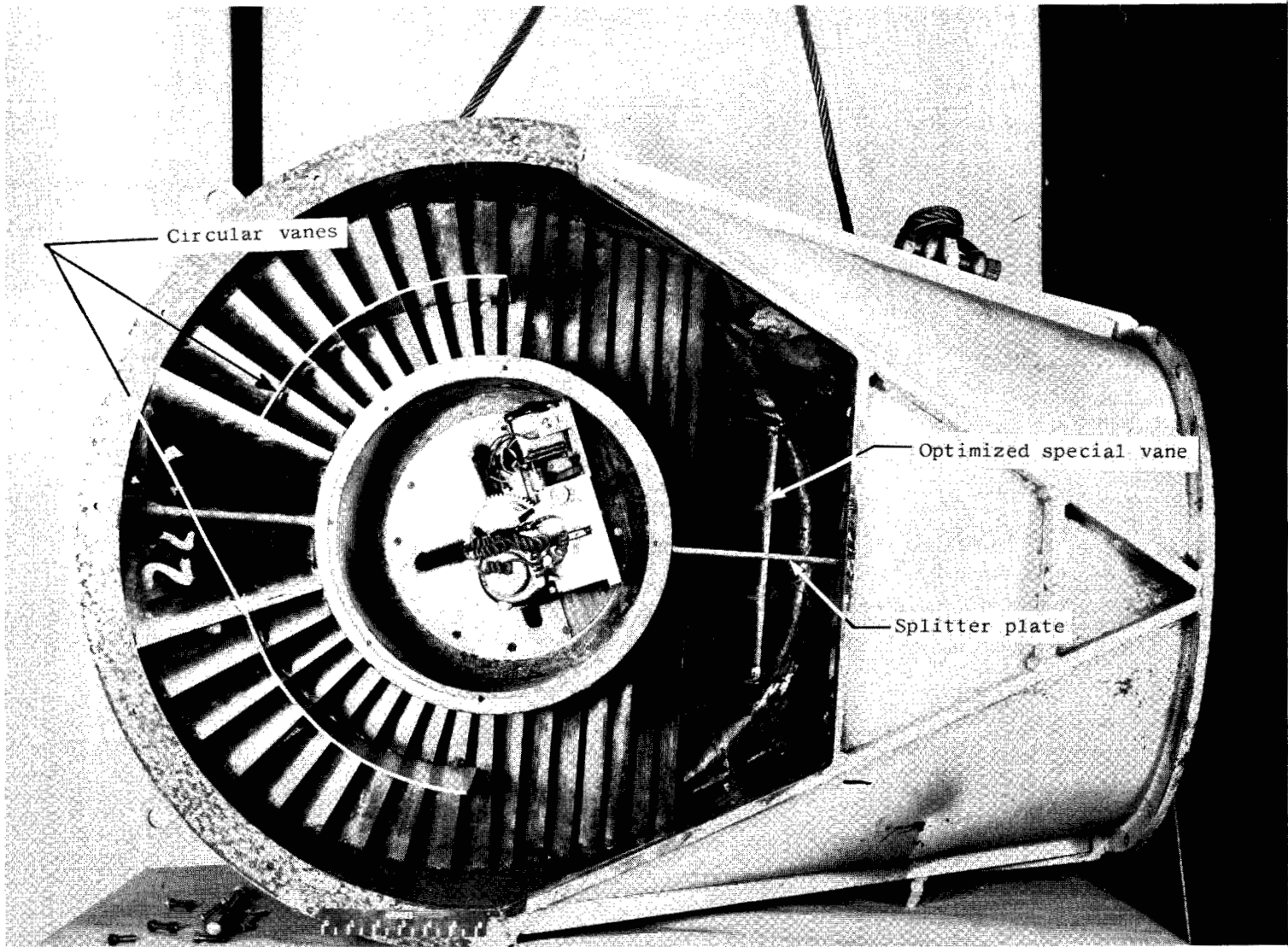
Figure 1.- Photographs of the elbow and turning vanes.



(b) Downstream end of elbow showing optimized special vane and splitter plate with exit nozzle removed.

L-58-910.1

Figure 1.- Continued.



(c) Interior view of vanes from upstream side showing the circular vanes.

L-58-905.1

Figure 1.- Concluded.

in.	cm
5.64	14.33
29.526	75.00
21.066	53.47
10.355	26.30
2.55	6.48
3.00	7.62
21.00	53.35
.64	1.625
.396	1.006
15.280D.	38.80D.
24.763D.	62.85D.
29.390D.	74.83D.
33.000D.	83.80D.

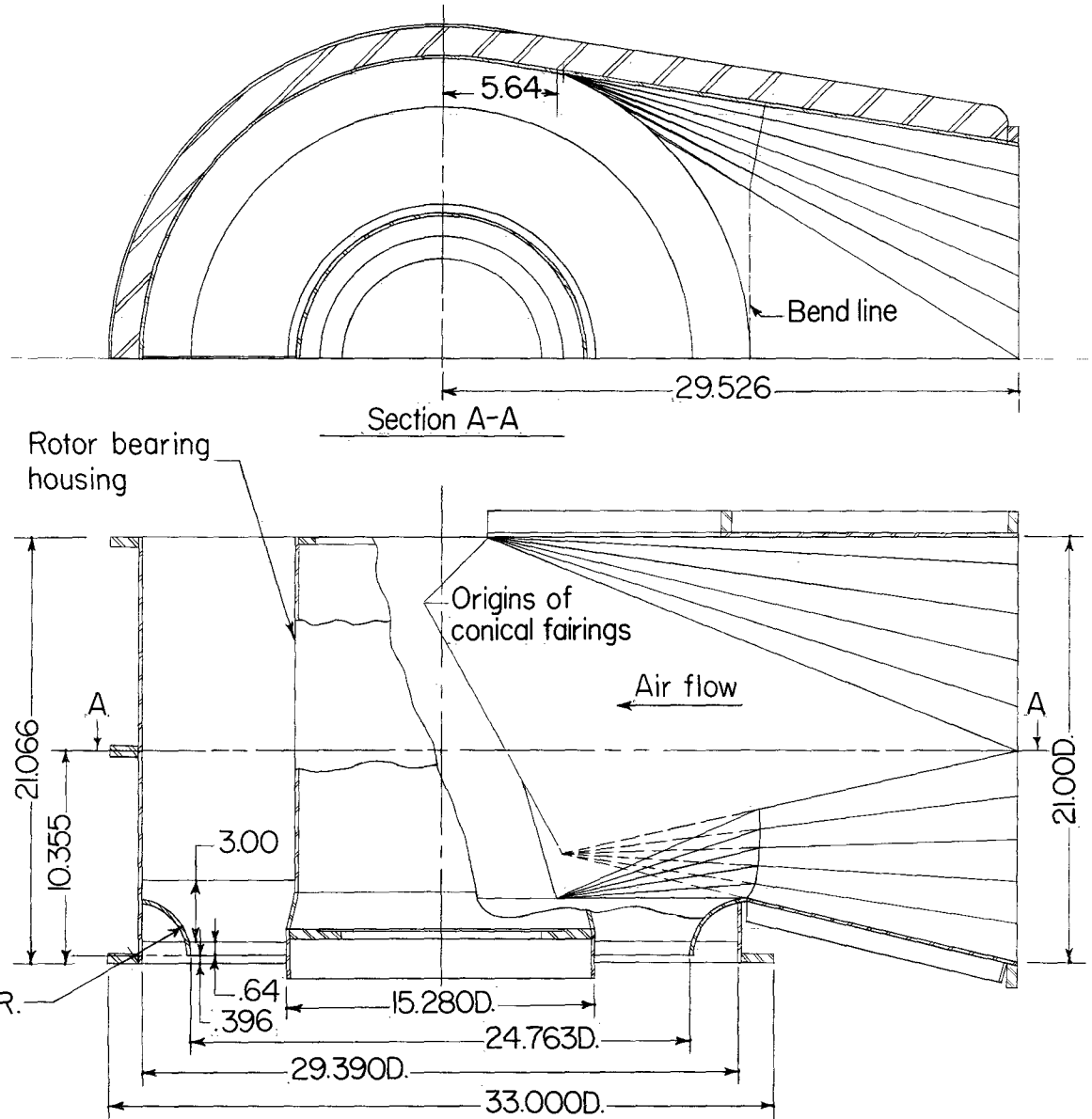


Figure 2.- Geometry of shell and center body of inlet elbow. All dimensions are in inches on the drawing and a table giving the dimensions in centimeters is included.

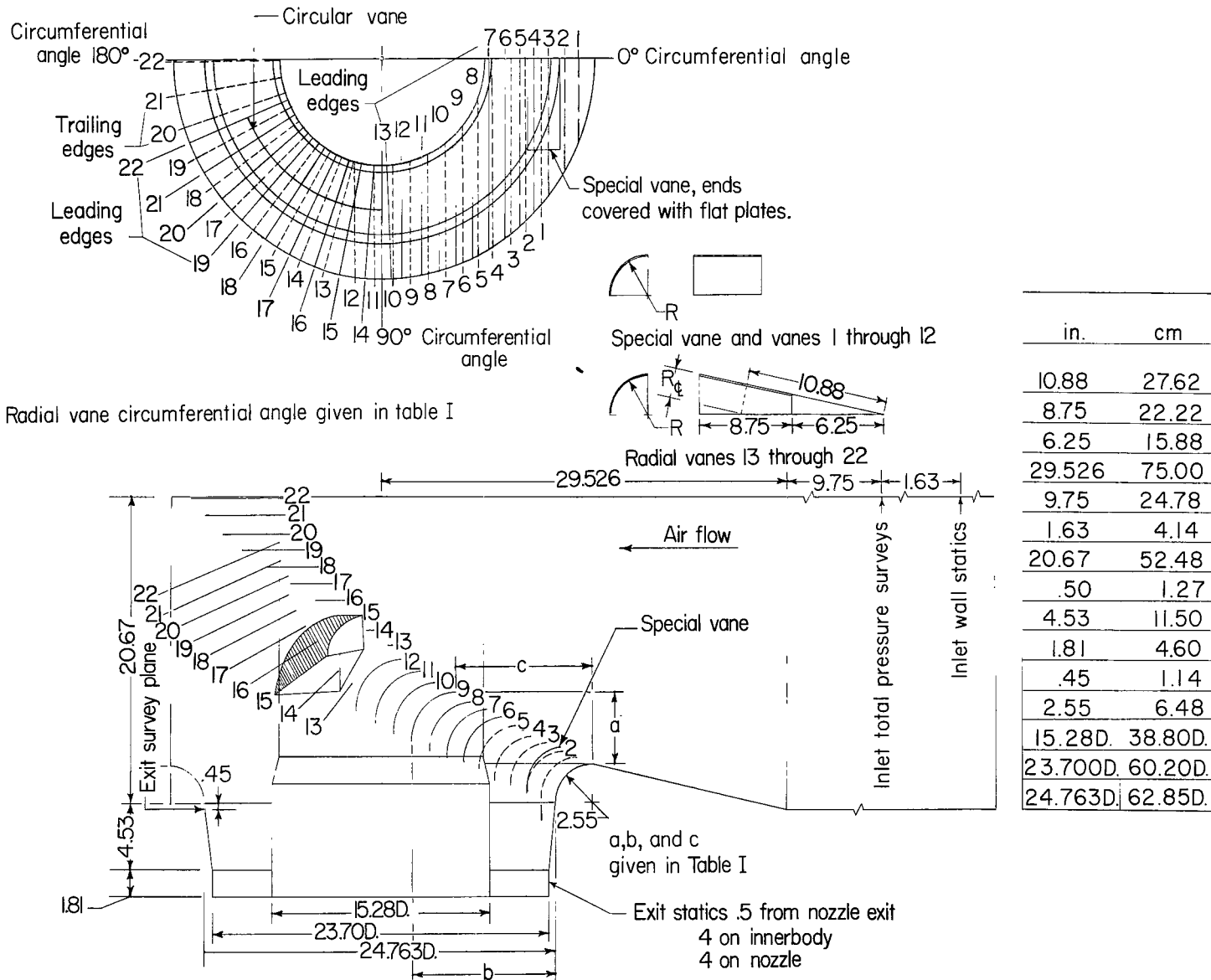


Figure 3.- Vane geometry and location in the inlet elbow and location of inlet and exit surveys and wall static-pressure orifices. All dimensions are in inches on the drawing and a table giving the dimensions in centimeters is included.

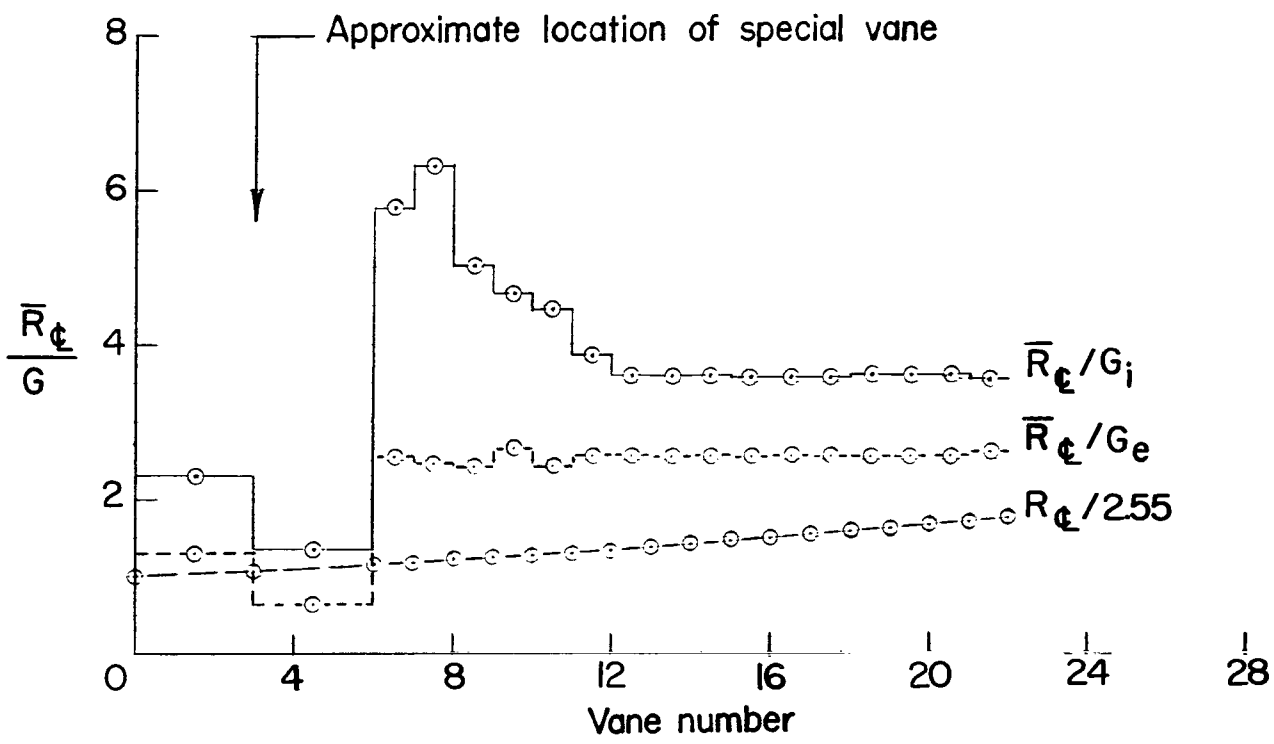
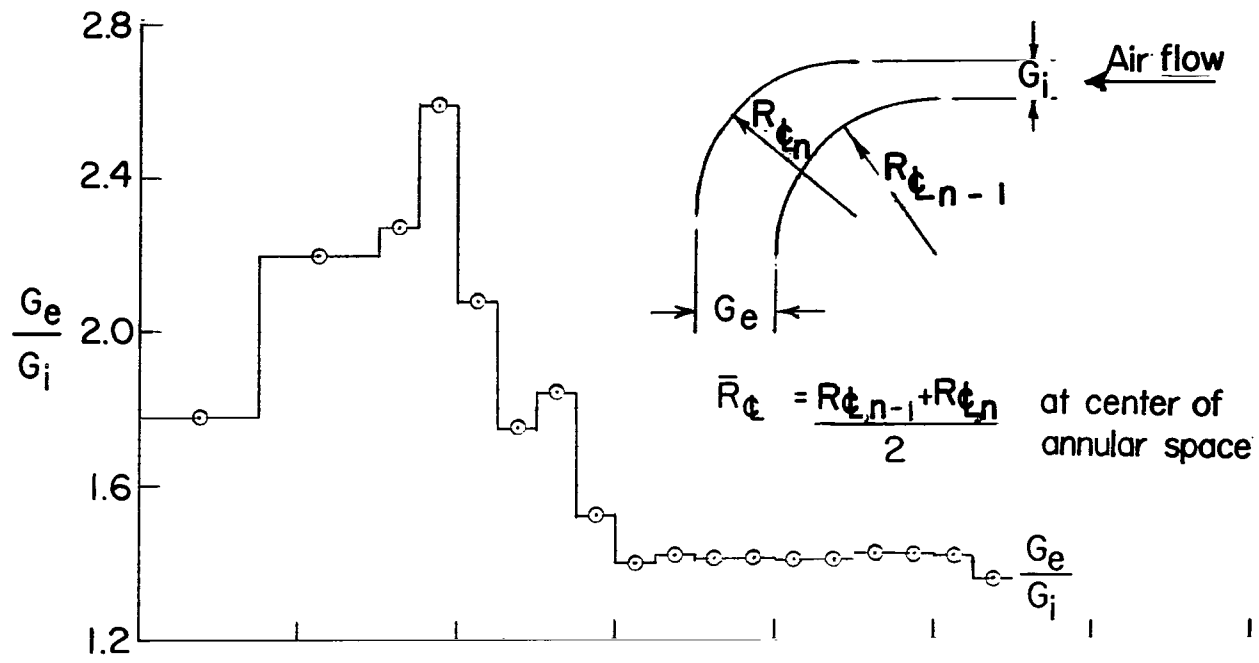
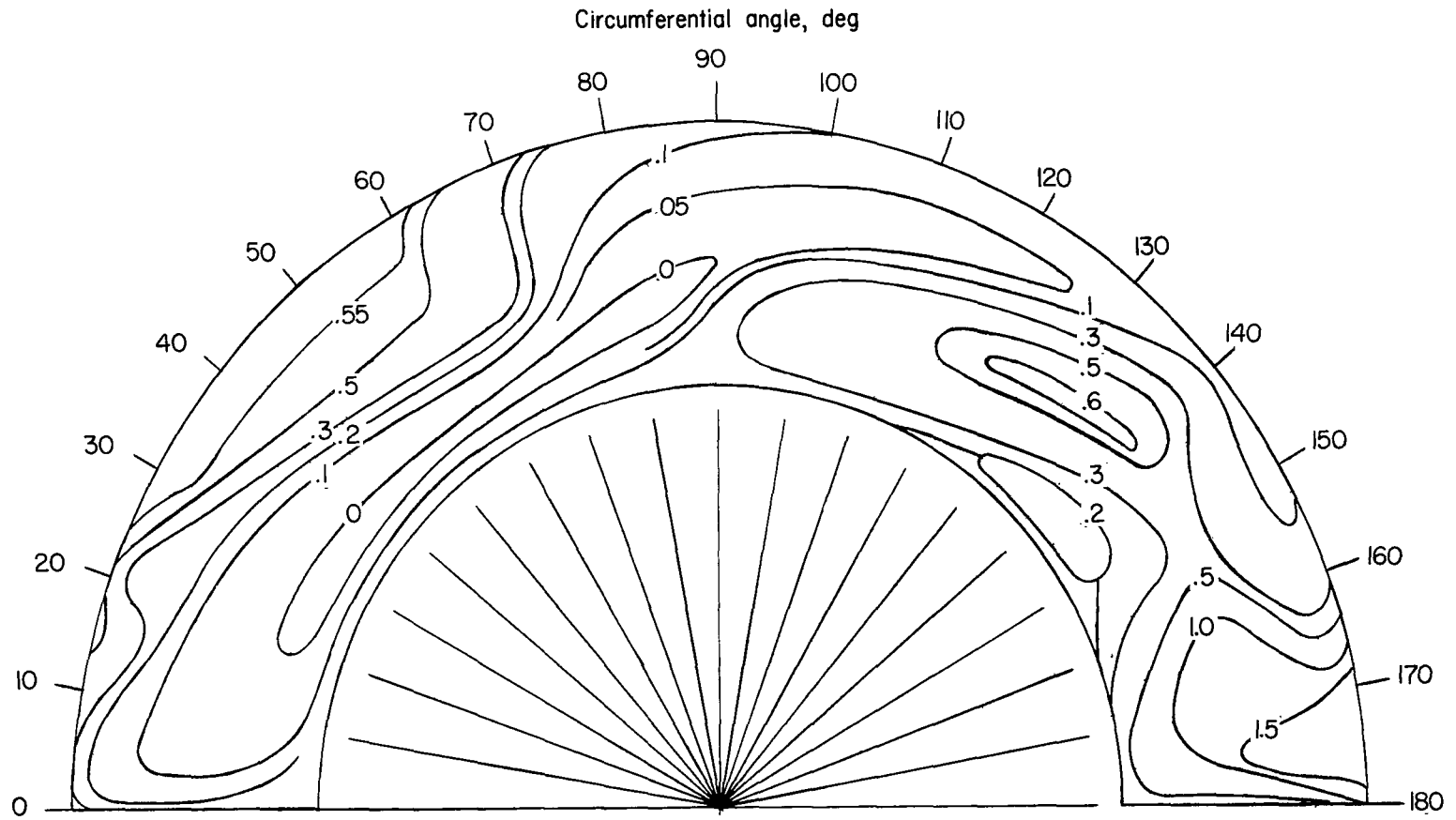
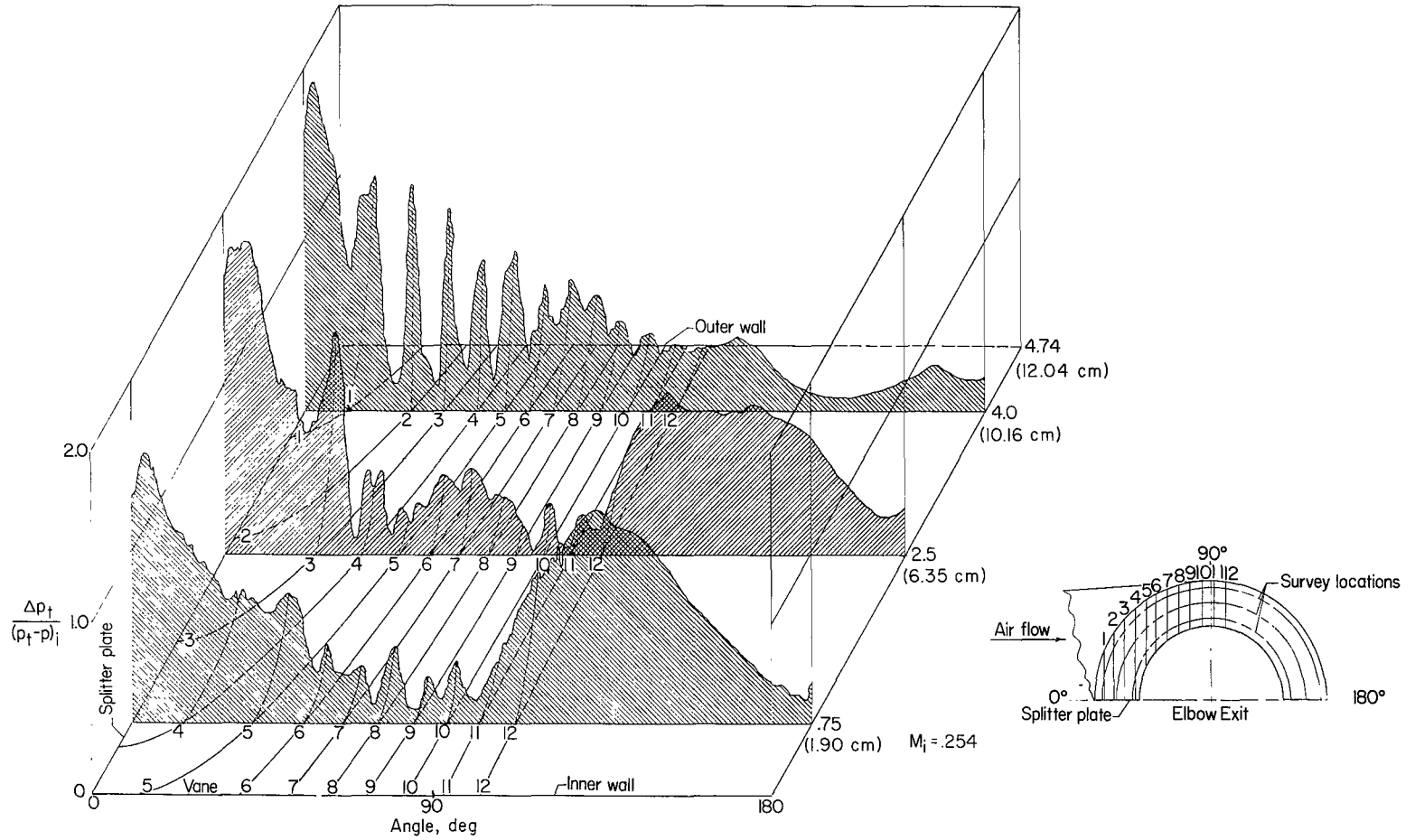


Figure 4.- Radius and gap ratios of vanes and vane passages.



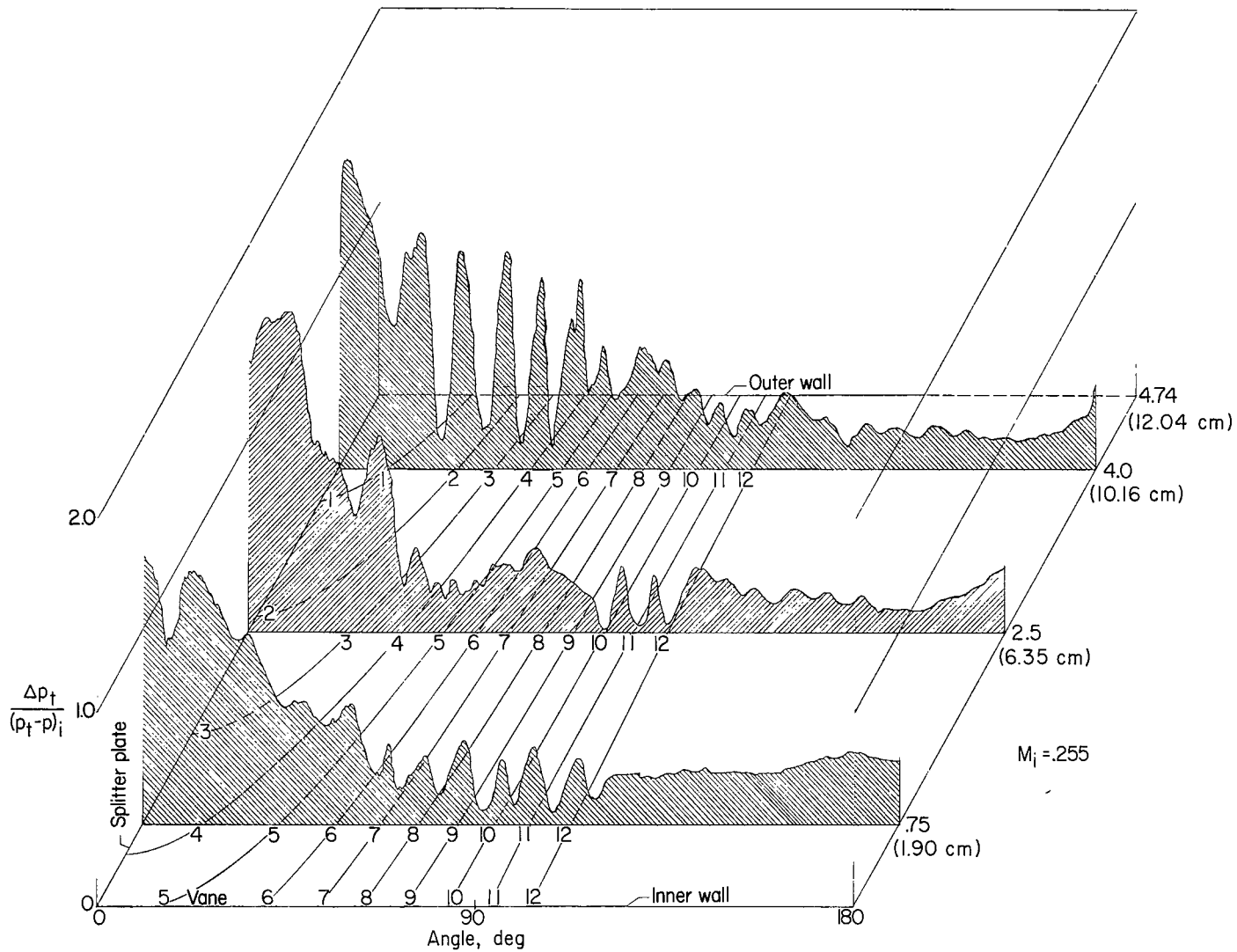
(a) No-vane condition.

Figure 5.- Exit loss coefficient $\frac{\Delta p_t}{(p_t - p)_i}$ contour maps for inlet elbow. Linear dimensions are in inches (cm).



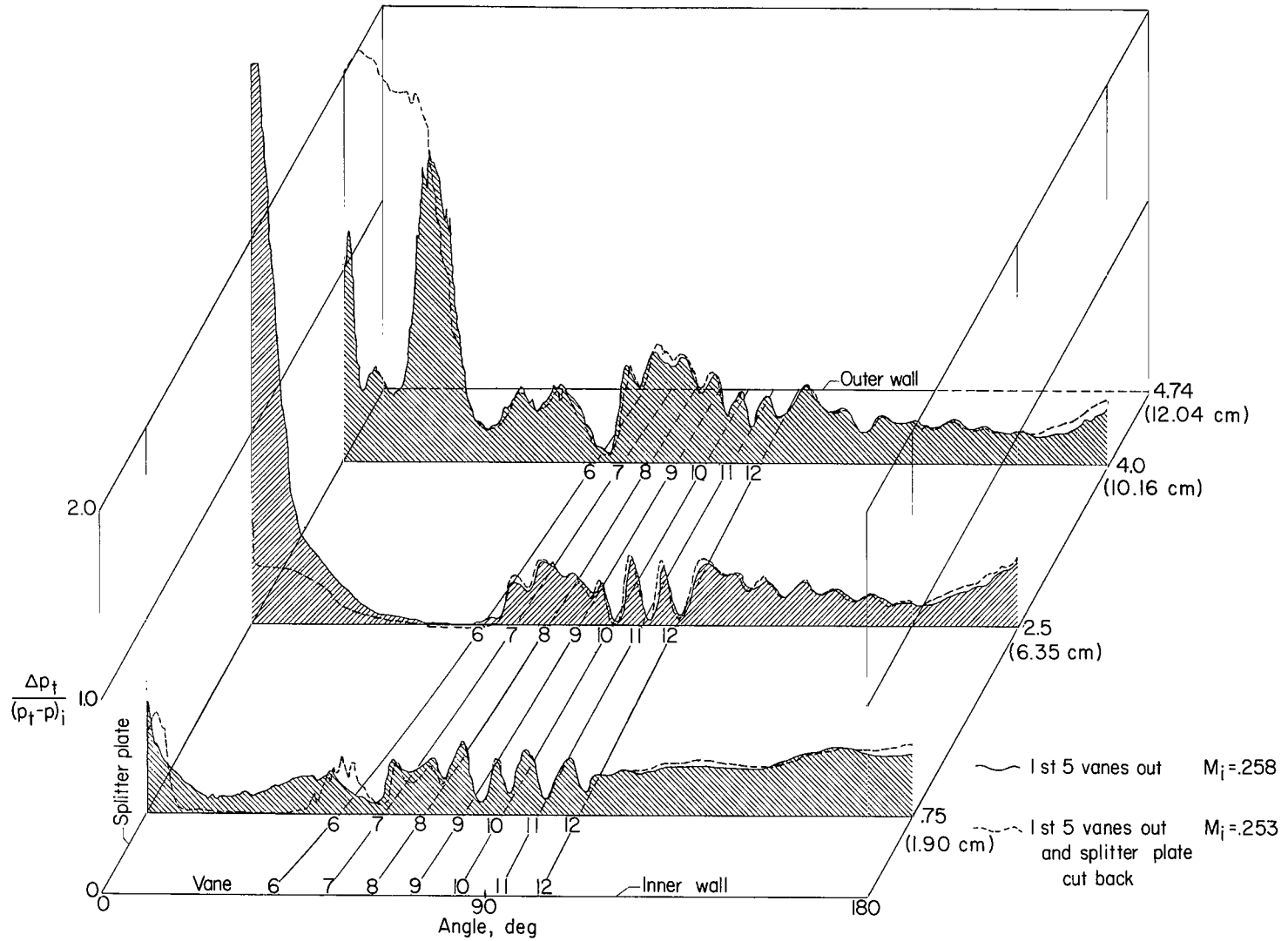
(b) Vane configuration 1, 12 straight vanes on inner half of elbow.

Figure 5.- Continued.



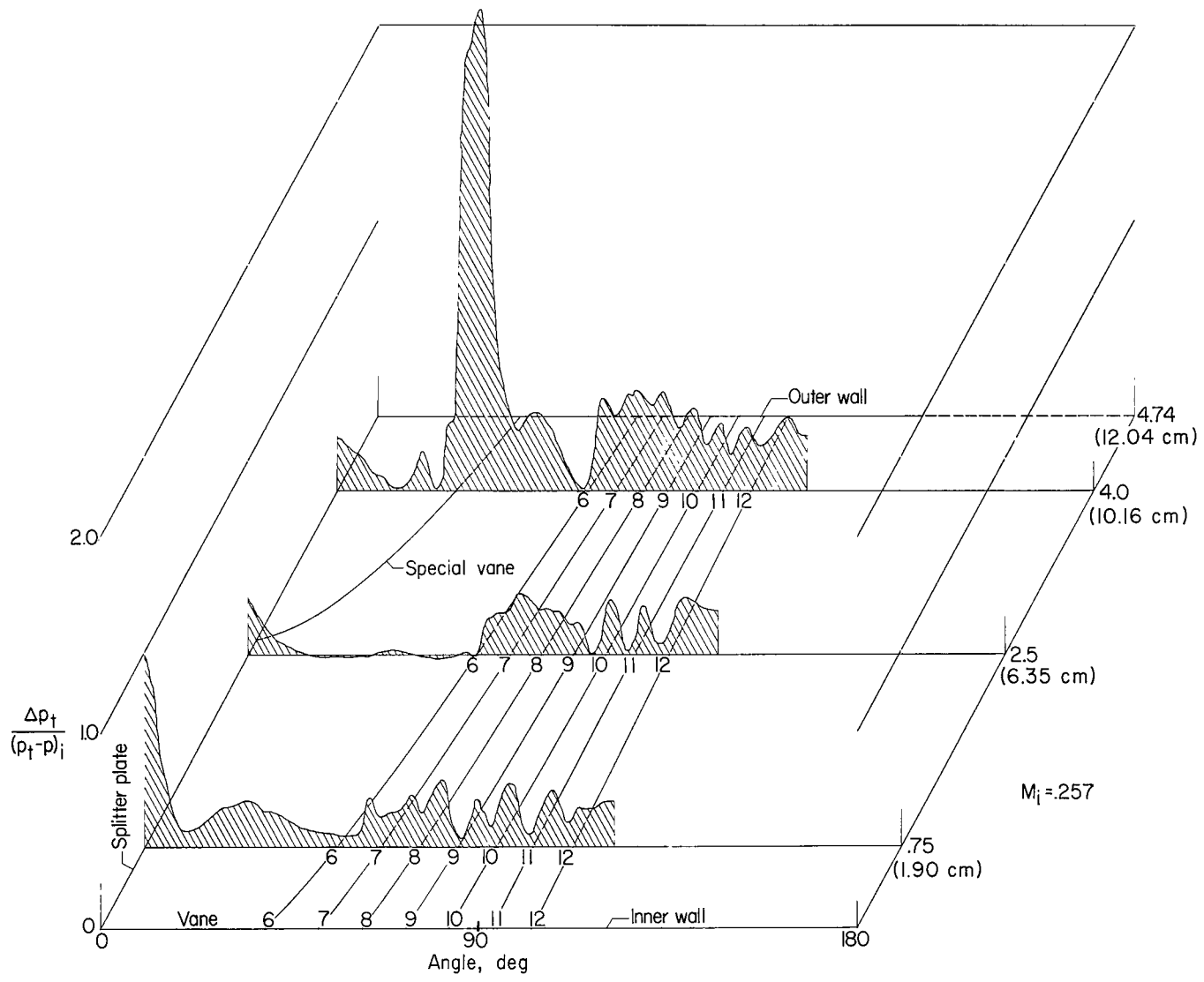
(c) Vane configuration 2, all vanes in.

Figure 5.- Continued.



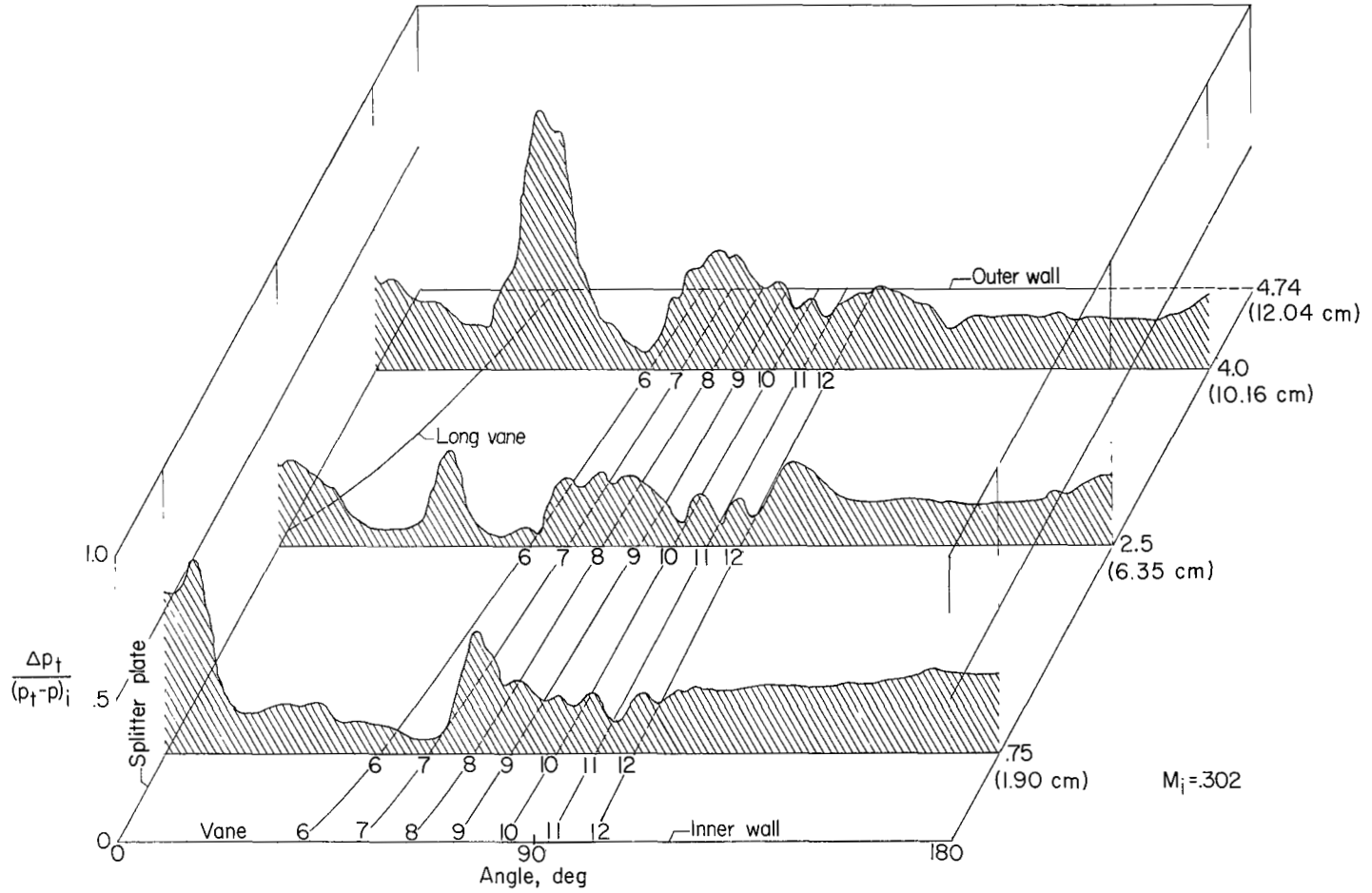
(d) Vane configuration 3, first 5 vanes out; vane configuration 4, first 5 vanes out and splitter plate cut back.

Figure 5.- Continued.



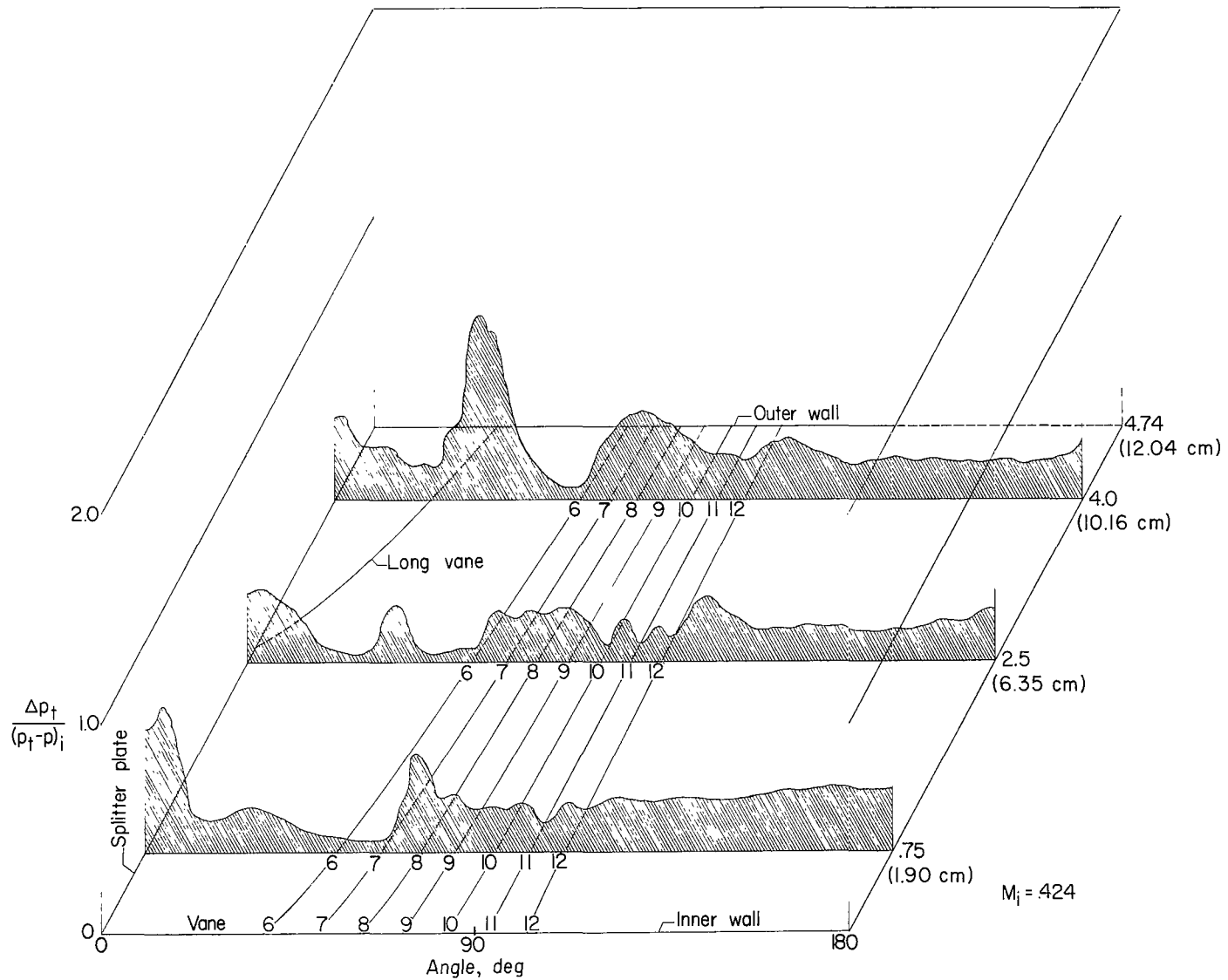
(e) Final vane configuration without an exit nozzle, vane configuration 10.

Figure 5.- Continued.



(f) Final vane configuration with an exit nozzle and diffuser, vane configuration 11. $M_i = 0.302$.

Figure 5.- Continued.



(g) Final vane configuration with an exit nozzle and diffuser, vane configuration 11. $M_i = 0.424$.

Figure 5.- Concluded.

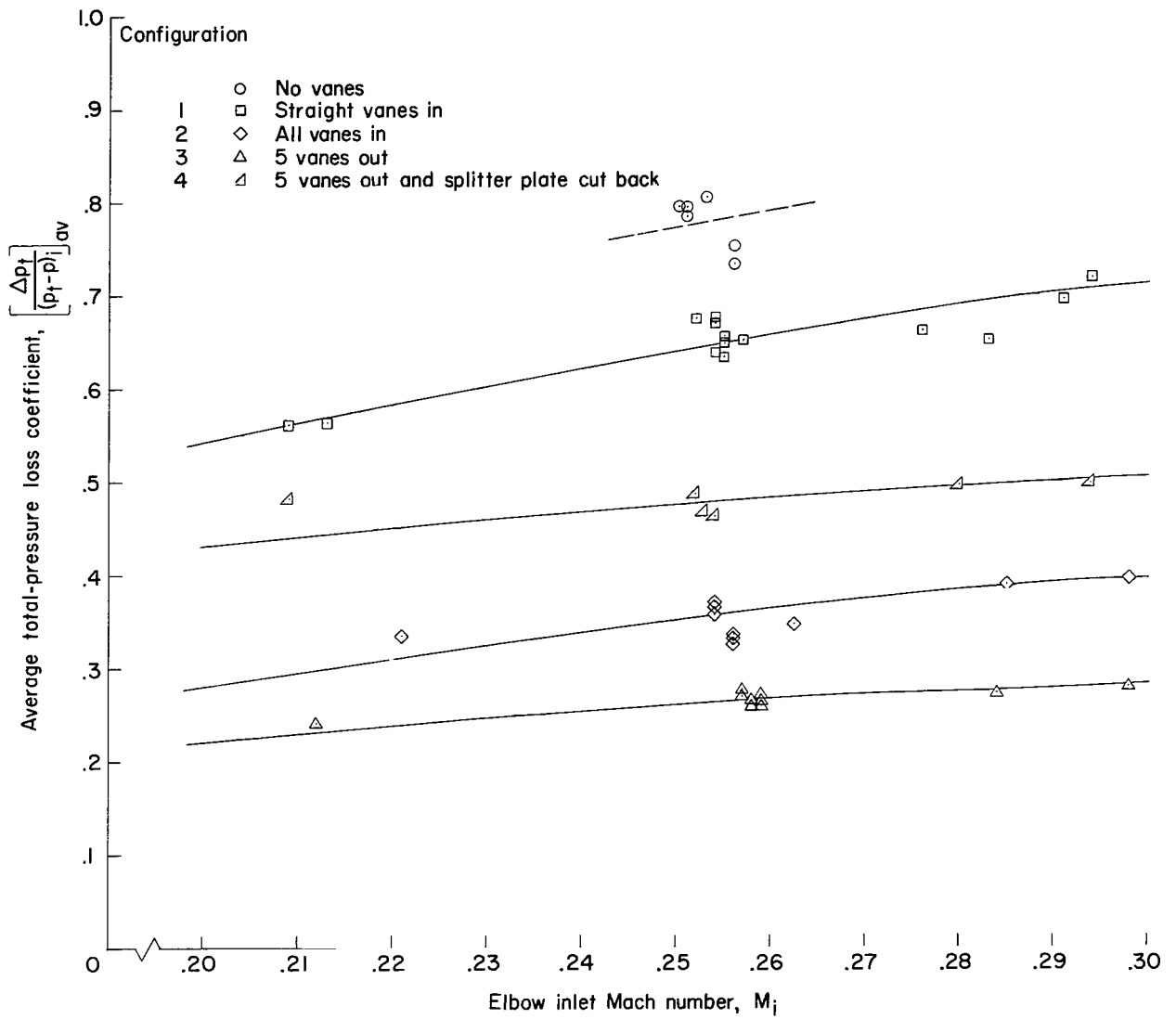


Figure 6.- Variation of average loss coefficient $\left[\frac{\Delta p_t}{(p_t - p)_{i,av}} \right]$ with elbow inlet Mach number for vane configurations 1 to 4 and the no-vane condition. (Average exit static pressure of configuration 10 was used.)

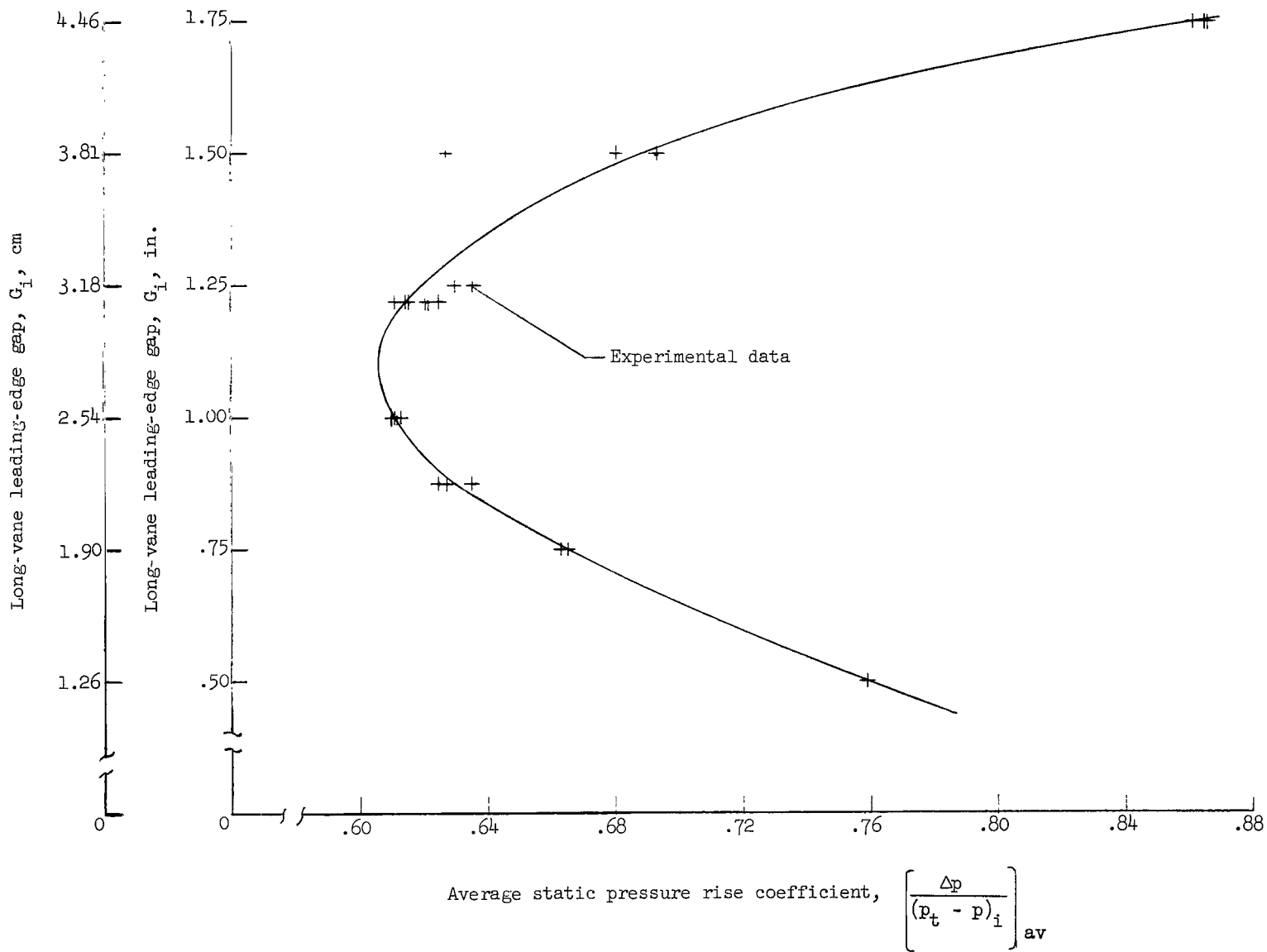


Figure 7.- Plot of average static-pressure rise coefficient against leading-edge vane gap to determine the optimum position of the special vane leading edge for use in the final vane configuration.

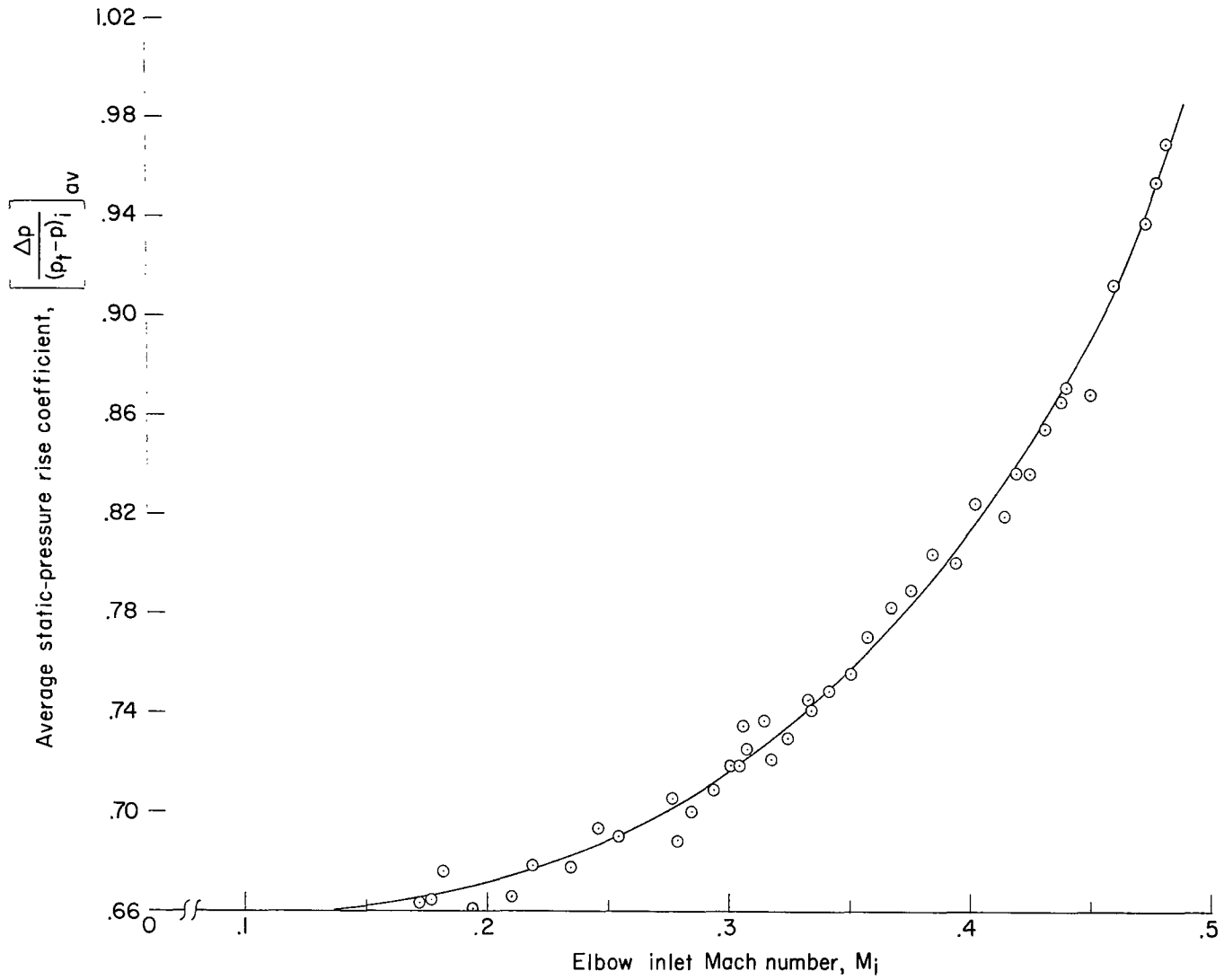


Figure 8.- Variation of average static-pressure rise coefficient $\left[\frac{\Delta p}{(p_t - p_i)} \right]_{av}$ with elbow inlet Mach number for optimized vane configuration.

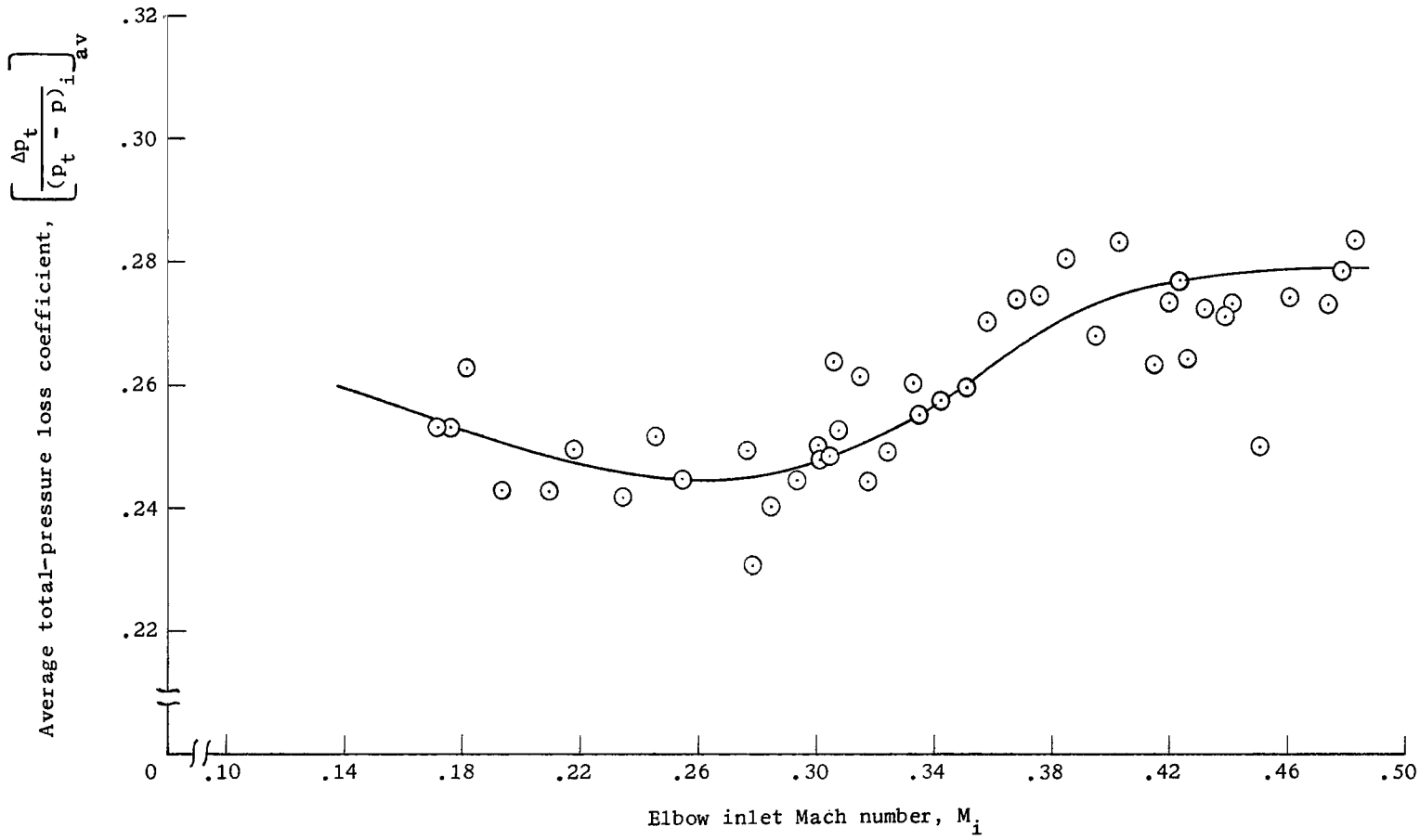


Figure 9.- Variation of average loss coefficient over a range of elbow inlet Mach numbers for vane configurations 10 and 11.

3/12/55
45

"The aeronautical and space activities of the United States shall be conducted so as to contribute . . . to the expansion of human knowledge of phenomena in the atmosphere and space. The Administration shall provide for the widest practicable and appropriate dissemination of information concerning its activities and the results thereof."

—NATIONAL AERONAUTICS AND SPACE ACT OF 1958

NASA SCIENTIFIC AND TECHNICAL PUBLICATIONS

TECHNICAL REPORTS: Scientific and technical information considered important, complete, and a lasting contribution to existing knowledge.

TECHNICAL NOTES: Information less broad in scope but nevertheless of importance as a contribution to existing knowledge.

TECHNICAL MEMORANDUMS: Information receiving limited distribution because of preliminary data, security classification, or other reasons.

CONTRACTOR REPORTS: Technical information generated in connection with a NASA contract or grant and released under NASA auspices.

TECHNICAL TRANSLATIONS: Information published in a foreign language considered to merit NASA distribution in English.

TECHNICAL REPRINTS: Information derived from NASA activities and initially published in the form of journal articles.

SPECIAL PUBLICATIONS: Information derived from or of value to NASA activities but not necessarily reporting the results of individual NASA-programmed scientific efforts. Publications include conference proceedings, monographs, data compilations, handbooks, sourcebooks, and special bibliographies.

Details on the availability of these publications may be obtained from:

SCIENTIFIC AND TECHNICAL INFORMATION DIVISION
NATIONAL AERONAUTICS AND SPACE ADMINISTRATION
Washington, D.C. 20546